USGS
science for a changing world

Prepared for the National Aeronautics and Space Administration

Geologic Map of MTM –15032 and –20032 Quadrangles, Western Ladon Basin, Mars

By Catherine M. Weitz, Sharon A. Wilson, John A. Grant, and Rossman P. Irwin, III

Pamphlet to accompany

Scientific Investigations Map 3525

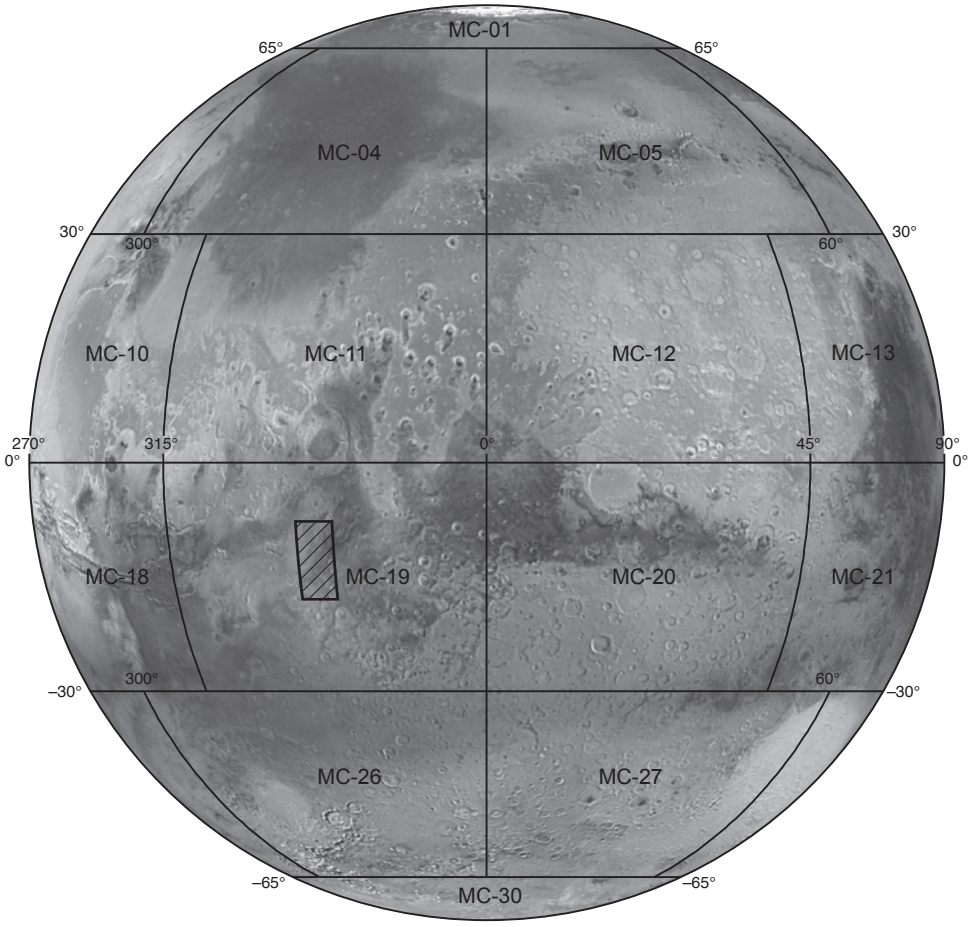

2025

U.S. Department of the Interior
U.S. Geological Survey

U.S. Geological Survey, Reston, Virginia: 2025

For more information on the USGS—the Federal source for science about the Earth, its natural and living resources, natural hazards, and the environment—visit https://www.usgs.gov or call 1–888–ASK–USGS.

For an overview of USGS information products, including maps, imagery, and publications, visit https://store.usgs.gov.

Any use of trade, firm, or product names is for descriptive purposes only and does not imply endorsement by the U.S. Government.

Although this information product, for the most part, is in the public domain, it also may contain copyrighted materials as noted in the text. Permission to reproduce copyrighted items must be secured from the copyright owner.

Suggested citation:
Weitz, C.M., Wilson, S.A., Grant, J.A., and Irwin, R.P., III, 2025, Geologic map of MTM –15032 and –20032 quadrangles, western Ladon basin, Mars: U.S. Geological Survey Scientific Investigations Map 3525, pamphlet 14 p., 1 sheet, scale 1:1,000,000, https://doi.org/10.3133/sim3525.

ISSN 2329-1311 (print)
ISSN 2329-132X (online)

Cover. Photomosaic showing location of map area (hachured rectangle). An outline of 1:1,000,000 scale quadrangles is provided for reference.

Contents

Table

Geologic Map of MTM –15032 and –20032 Quadrangles, Western Ladon Basin, Mars

By Catherine M. Weitz,[1] Sharon A. Wilson,[2] John A. Grant,[2] and Rossman P. Irwin, III[2]

Introduction

Ladon basin is located in the western equatorial region of Mars in Margaritifer Terra (fig. 1, map sheet). The western part of Ladon basin and its bounding basin ring structures to the west preserved features that help to understand the long history of drainage across the Margaritifer Terra region of Mars. Recent and ongoing studies have placed important constraints on water-driven degradation of the informally named Ladon and Holden basins, Ladon and Uzboi Valles, Holden crater, Eberswalde crater, and numerous intracrater alluvial fans in the area (Pondrelli and others, 2005, 2008; Grant and others, 2008, 2010a; Irwin and Grant, 2009, 2013; Grant and Wilson, 2011, 2012). In addition, preliminary analysis of Ladon Valles, Ladon basin, and Ladon highland sediments (Milliken and Bish, 2010; Weitz and Bishop, 2012; Weitz and others, 2013, 2019, 2022) suggests that the intervening area and the western side of Ladon basin may provide additional details regarding the aqueous conditions and extent of sedimentary deposition when water was flowing on the surface. Margaritifer Terra preserves an extensive assembly of features related to aqueous degradation (for example, Carr, 1981; Baker, 1982; Moore and Howard, 2005), and it is an ideal location for mapping focused on defining stratigraphy and additional morphologic and morphometric details of valleys and fluvial or alluvial deposits.

Previous mapping, and especially mapping by Irwin and Grant (2013), identified the degraded Ladon and Holden multi-ringed impact basins (Schultz and others, 1982) as the oldest features. Their ring structures are now isolated mountains mostly fringed by a broad, gently sloping expanse of rock debris and aprons. The most widespread unit in areas mapped to date is the Middle Noachian highland unit (mNh in Tanaka and others, 2014), which includes basaltic bedrock (Bandfield and others, 2000), impact ejecta, weathered rocks (Murchie and others, 2009), fluvially reworked sediments, and eolian materials. Fluvial dissection is common on slopes, and layering is evident in some places. Highland unit surfaces infill and embay older Noachian craters but have also been disrupted by younger craters. They do not retain small crater structures (<1 kilometer [km] diameter) as well as the smooth basin fills (Malin, 1976; Malin and Edgett, 2001).

Both the Ladon and Holden impact basins include a thick fill unit that is sometimes stratified (Grant and Parker, 2002) and is interpreted as moderately to strongly indurated alluvial, volcanic, and (or) eolian materials, where origin and composition likely vary within and between basins (Irwin and Grant, 2013). In addition, clay-bearing layered outcrops are found in Holden and Eberswalde craters, southern Ladon basin, northern Ladon Valles, and several small upland basins west of Ladon basin (Pondrelli and others, 2005, 2008; Lewis and Aharonson, 2006; Grant and others, 2008; Milliken and Bish, 2010; Rice and others, 2011; Weitz and Bishop, 2012; Thomas and others, 2017; Weitz and others, 2019, 2022), suggesting that their depositional environments could be similar. Beds in the clay-bearing deposits are often less than a meter thick, can be traced for hundreds of meters, and do not appear to truncate one another. The deposits are mostly confined to low elevations and do not drape exterior surfaces, favoring low-energy alluvial, fluvial, or lacustrine deposits rather than airfall materials, such as volcanic ash.

Although previous mapping of eastern Ladon basin by Irwin and Grant (2013) provided some insight into the role of water in this region, especially the development of Ladon Valles in the south, sediments transported through Ladon Valles and deposited into western Ladon basin were not part of their mapping. Hence, a critical aspect of the aqueous history and sedimentary record for the middle section of the Uzboi-Ladon-Morava (ULM) mesoscale outflow system remained unaddressed. Similarly, the mapping of Morava Valles by Wilson and others (2022) provided important results about geologic processes and the geologic history at the terminus of the ULM system, but it did not include the area between Ladon Valles and Morava Valles. Consequently, our mapping of western Ladon basin fills a critical gap in the ULM system needed in order to define the influence of the outflow system in the landscape evolution of the Margaritifer Terra region.

In addition, although previous mapping has provided a wealth of new information about the light-toned layered deposits in Holden and Eberswalde craters, the relationship of these deposits to the newly identified deposits within and around western Ladon basin remain unknown. Whether the layered deposits in Holden crater, Eberswalde crater, Ladon basin, Ladon Valles, and other depressions are linked in time or process is currently uncertain, but their similar properties suggest a connection to water-driven processes. Layered deposits in Holden and Eberswalde craters are in enclosed basins, whereas deposits near the mouth of Ladon Valles and on the western

[1]Planetary Science Institute.

[2]Smithsonian Institution.

flank of Ladon basin are currently in open basins, although that might not have been the case when they were deposited. Most of the clay-bearing sediments may have been derived upstream from the surrounding weathered Noachian highlands and later transported into the basins (Milliken and Bish, 2010; Weitz and others, 2022), although some may have been produced by weathering of the basin materials. Nevertheless, while the origin of clays in the layered deposits is ambiguous, it likely reflects environments subjected to prolonged chemical weathering. Because the clays occur in stratified, apparently sedimentary rocks, they may provide evidence to whether past depositional settings were ever habitable (Grant and others, 2008; Milliken and Bish, 2010; Thomas and others, 2017).

The goal of this mapping project is to define the evolution of the western Ladon basin (fig. 1) as it relates to fluvial and (or) alluvial events that occur on surrounding surfaces to constrain the extent and causes of sedimentary deposition and aqueous alteration in Margaritifer Terra. Our geologic map provides new insight into the extent of aqueous activity across western Ladon basin and the adjoining highlands, which includes the northern part of Ladon Valles, Arda Valles, numerous small valleys in the western highlands, and light-toned layered deposits associated with these fluvial features. Our mapping fills a key gap in our knowledge about the geologic setting of the Margaritifer Terra region and connects mapping to the east and south by Irwin and Grant (2013) with mapping to the northeast by Wilson and others (2022).

Physiography and Background

Our mapping focused on the geomorphic terrains and geologic units contained within Mars Transverse Mercator (MTM) −15032 and −20032 quadrangles (fig. 1). These two quadrangles are located along the west side of Ladon basin and span lat −12.5 to −22.5° N. and long 325 to 330° E. The map area contains impact craters of a wide range of sizes that display a variety of erosional states. Some craters exhibit well-preserved lobate ejecta deposits with defined margins and meter-scale topography, whereas others are almost completely buried or eroded. Several of the craters are filled by deposits that have undergone extensive fracturing.

Ladon basin is a large impact basin that was partly disrupted by the younger Holden basin centered to the southwest (Schultz and others, 1982; Grant, 1987) and is incised by the ULM mesoscale outflow system (Grant and Parker, 2002; Irwin and Grant, 2009, 2013) (fig. 1). The floor of Ladon basin is horizontal with a maximum relief of 300 meters (m) over 350 km (excluding craters). The basin is ringed by mountains that have shed sediments through a radial, centripetal network of valleys that are broad and deeply incised (for example, Arda Valles, see Grant, 1987). Nevertheless, discrete deposits near the mouths of the valleys remain difficult to identify. Much of the terrain within and adjacent to our map area has been mapped as the terra unit (Irwin and Grant, 2013; Wilson and others, 2022), which was previously mapped as the cratered unit by Scott and Tanaka (1986) and the cratered plateau materials by Saunders (1979). The unit is widespread in the southern highlands and appears as an uneven, cratered surface with moderate relief. These materials are interpreted to have a sedimentary, impact, and (or) volcanic origin (Saunders, 1979; Scott and Tanaka, 1986; Grant and Parker, 2002; Irwin and Grant, 2013); were emplaced during resurfacing events; and bury much of the cratered highlands surrounding Ladon and Holden basins. A subdued crater unit was previously mapped within Ladon basin (Saunders, 1979; Scott and Tanaka, 1986), although the basin itself was never identified. More recent mapping of eastern Ladon basin by Irwin and Grant (2013) subdivided the basin fill into three different units: HNb_1, HNb_2, and Hb_3.

To the south and continuing into our map area are the channel units of Ladon Valles. Broader, sinuous channels initially dissected much of northern Holden basin and southern Ladon basin before the flow coalesced and downcut the main channel that now makes up Ladon Valles. Numerous valleys that are part of Arda Valles dissect the terrain at the juncture between northern Holden and southwestern Ladon basins. The valleys of Arda Valles are oriented southwest to northeast, which is radial to Ladon basin, indicating that the local topography of Ladon basin rather than Holden basin influenced the water flow in this region.

The ejecta surrounding the Hesperian (3.0–3.5 giga-annum [Ga] using Hartmann and Neukum, 2001) Holden crater (lat −26.0° N., long 325.8° E.) and Ostrov crater (lat −26.5° N., long 332° E.) postdate these units and resurfaced much of the area south of Ladon basin (Mangold and others, 2012; Irwin and Grant, 2013). Secondary craters from Holden extend well beyond the continuous ejecta and cover many surfaces within and west of Ladon basin, creating a regional stratigraphic marker for determining the relative age of surfaces.

Late Noachian–Early Hesperian channel materials of Uzboi, Ladon, and Morava Valles include exposed bedrock outcrops, eroded highland outcrops, and alluvial veneers (Irwin and Grant, 2013). At least three periods of fluvial activity occurred from the Noachian into the Amazonian. These periods include (1) early incision of the ULM system from 3.5–3.8 Ga and partial filling of Ladon basin (Grant and Parker, 2002); (2) later activity depositing the clay-bearing sediments in Holden crater and Uzboi Vallis and possibly near the mouth of Ladon Valles (Grant and others, 2008, 2010b); and (3) alluvial fan deposition throughout Margaritifer Terra (Grant and Wilson, 2011, 2012), including two craters within our map area. Argyre basin, southwest of the map area, is the interpreted source of water that carved out the ULM system and likely formed in the Early to Middle Noachian (Hiesinger and Head, 2002; Werner, 2008; Fassett and Head, 2011; Robbins and Hynek, 2012), but the timing of initial incision of the ULM mesoscale outflow system and the last through-flowing discharge along the ULM system and into Ladon basin remains uncertain. Discharge, as evidenced by the overflowing of both Holden and Ladon basins (Parker and Pieri, 1985a), occurred before the system was interrupted by Hale, Bond, and Holden craters, but when discharge occurred and the extent of flooding in Argyre basin provide clues as to when and why Ladon basin became degraded. The likely Amazonian age of Hale crater (Cabrol and others, 2001; Jones and others, 2011) and Hesperian age of Holden crater (Mangold and others, 2012; Irwin and Grant, 2013) constrain the last period of water flow into Ladon from the south.

Incision of Ladon Valles likely occurred during multiple large discharge events (Grant and Parker, 2002; Irwin and Grant, 2013) from filling and overflowing of Holden basin. The

discharges from Holden basin were so large that the pre-valley topography could not initially confine the flow(s) into a single channel. The hanging side channels and the main stem suggest that multiple overflow points remained active until the central channel was incised deeply enough to confine the entire flow. These observations are consistent with at least five distinct terraces along Ladon Valles (Boothroyd, 1983; Parker and Pieri, 1985a; Grant, 1987; Grant and Parker, 2002). Discharge estimates during incision of the ULM system are somewhat uncertain, but the elevation of terraces along Ladon Valles, combined with the cross-section dimensions and gradient of the channel, suggest discharge rates between 150,000 cubic meters per second (m^3/s) and 450,000 m^3/s (Grant and Parker, 2002).

Although discharge out of Ladon Valles was at least occasionally quite great (Irwin and Grant, 2009), whether the events were characterized by relatively sediment-free versus sediment-laden water flow is poorly understood. Thick outcrops with limited stratification located at the mouth of Ladon Valles are consistent with fewer but sediment-laden discharge events. By contrast, numerous finely bedded strata are more consistent with frequent sediment-poor discharge and (or) ponding within Ladon basin prior to establishment of the Morava Valles outlet.

The final water-driven geomorphic activity in southwest Margaritifer Terra involved deposition of alluvial fans within some craters that included nearby Holden, Eberswalde, and Ostrov craters (Grant and Wilson, 2021) and two craters in the map area (Alnif crater at lat −15.1° N., long 328.9° E. and an unnamed crater at lat −15.9° N., long 328.3° E.; see Wilson and others, 2021). Alluvial fan deposition in surrounding areas was active in the Late Hesperian to Early Amazonian (~3.0 Ga) (Grant and Wilson, 2011). Grant and Wilson (2012) interpreted alluvial deposition to be related to synoptic to globally occurring precipitation, perhaps as snowfall, which accumulated in crater-rim depressions and later melted to produce runoff.

Base Map and Data

The datasets described below were compiled and analyzed in a geographic information system (GIS) project. Linework was drafted at 1:250,000 scale for publication at 1:1,000,000 with stream-digitized vertex spacing of ~250 m. We used several image and topographic datasets for mapping and analyses of western Ladon basin, Ladon Valles, and the surrounding highlands. The suite of image datasets provides complementary spatial coverage over a wide range of spatial resolution (~1–100+ meters per pixel [m/pixel]), allowing surface characterization at several geologically relevant scales. The primary base map used for this geologic map is composed of daytime thermal infrared (IR) images acquired by the Thermal Emission Imaging System (THEMIS) camera (Christensen and others, 2004) on the Mars Odyssey spacecraft and compiled into a 100 m/pixel mosaic (Fergason and others, 2013) (fig. 2, map sheet). We also used a THEMIS nighttime mosaic (100 m/pixel) to evaluate thermal inertia properties of the geologic units. The geologic units that are mapped and described herein are geodetically tied to the THEMIS daytime base map.

We used other data sets to discern geologic unit boundaries and provide additional characteristics about the geologic units, such as composition and evidence for stratification. We used a topographic map (fig. 2) from gridded data collected by the Mars Orbiter Laser Altimeter (MOLA) (128 pixels per degree or ~463 m/pixel resolution) (Smith and others, 2001), an instrument on Mars Global Surveyor (MGS), to analyze topographic characteristics and help understand superposition and embayment relations between geologic units. The Mars Reconnaissance Orbiter (MRO) panchromatic and color High Resolution Imaging Science Experiment (HiRISE) images (~0.25–0.5 m/pixel resolution) (McEwen and others, 2007) provided additional characteristics about the geologic units, such as layering within sedimentary deposits. Individual MRO Context Camera (CTX) images were mosaicked by the Murray Laboratory at the California Institute of Technology (http://murray-lab.caltech.edu/CTX/index.html) into tiles that covered the entire map area at ~6 m/pixel resolution (Malin and others, 2007; Dickson and others, 2018). We used the CTX mosaics to discern geologic unit boundaries, identify light-toned deposits and other features not covered by HiRISE or discernable in the THEMIS IR base map, and determine crater diameter measurements.

Finally, we analyzed the MRO Compact Reconnaissance Imaging Spectrometer for Mars (CRISM) hyperspectral data to provide mineralogical interpretation of deposits on the floor of Ladon basin, within Ladon Valles, and in the highland basins. CRISM collects ~10-km-wide images from 0.36 to 3.92 micrometers (μm) at 18 m/pixel in the full-resolution targeted mode (FRT) and at 36 m/pixel in the half-resolution short (HRS) or long (HRL) mode (Murchie and others, 2007). The CRISM images are available in the Planetary Data System (PDS), https://pds-geosciences.wustl.edu/missions/mro/crism.htm.

Methodology

We constructed the geologic map of western Ladon basin at 1:1,000,000 scale according to the methods described by Tanaka and others (2011) and Skinner and others (2022). We applied basic planetary mapping principles (for example, Greeley and Batson, 1990; Tanaka and others, 1994, 2011) to define map units based on topography, morphology, stratigraphic relations, and relative age. The designated unit names are descriptive where unique primary morphology was evident (for example, fan unit, chaotic unit, volcanic unit) but we named other units with more ambiguous origin and (or) composition on the basis of their geographic and stratigraphic locations (for example, basin fill 1 unit is older than basin fill 3 unit) after Irwin and Grant (2013). Below, we describe (1) digital drafting parameters used to compile information, (2) unit groups, names, and symbols, (3) types of geologic contacts, and (4) types of feature symbols.

Digital Drafting Parameters

We digitized contact, line, and polygon features using a GIS at a scale of 1:250,000, to ensure line fidelity and the publication map scale of 1:1,000,000, which allowed for substantially detailed

lines for use in both printed and digital publications. We used geologic map symbols from the "FGDC Digital Cartographic Standard for Geologic Map Symbolization" (Federal Geographic Data Committee, 2006) and adapted them, where necessary, to convey the geologic information unique to the quadrangles. Iterations of the digitized linework allowed refinement of contact placement and unit descriptions on the basis of cross-comparison between the map base and supplemental data sets. We cleaned the contact linework (for example, dangles removed) and used them to build unit polygons.

Unit Groups, Names, and Labels

Geologic unit groups are similar to and consistent with those mapped by Irwin and Grant (2013) and Wilson and others (2022) and include (1) impact crater units, (2) chaotic units, (3) volcanic units, (4) basin fill units, (5) crater, valley, and channel units, and (6) plateau and highland units. We named the units based on their geographic occurrence as well as their stratigraphic relations to one another. We identified twenty geologic units in the map area: three units within the impact crater group (HNc_1, Hc_2, and AHc_3); one unit within the volcanic group (Av); one unit within the chaotic group (Act); six units within the basin fill group (HNb_1, HNb_2, HNb_3, AHb_4, AHlb, and AHb_5); six units within the crater, valley, and channel group (Nch_1, $HNch_2$, Hcf, AHlc, AHlh, and Af); and three units within the plateau and highland group (Nm, Nt_1, and Ht_2).

We assigned a label to each map unit that uniquely identifies the chronologic period(s) in capital form (N, Noachian Period; H, Hesperian Period; and A, Amazonian Period). We used a numerical subscript to identify the interpreted stratigraphic order for closely related units (for example, 1, the oldest of two or more sequentially emplaced units) or primary emplacement morphology (c, crater unit; v, volcanic unit; ct, chaotic terrain; b, basin fill unit; ch, channel unit; cf, crater fill unit; l, light-toned unit; h, highland unit; f, alluvial fan unit; m, mountainous unit; and t, terra unit).

Contact Types

We delineated the geologic units within the map area using contacts that we attributed with their interpreted level of certainty and their geologic occurrence. A "certain" contact denotes the most precise contact between well-characterized geologic units that contrast in appearance and (or) interpreted relative age. An "approximate" contact denotes less precise unit placement on the basis of diffuse, gradational, and (or) obscured unit boundaries. Internal contacts within crater units of the same age were used to show age relationships between overlapping ejecta where clear superpositioning or embayment relationships exist.

Feature Types

The map includes a variety of morphologic feature symbols, following precedents established in previous terrestrial and planetary geologic maps. Mapped linear features include wrinkle ridges, scarp crests, fluvial channels, crests of exposed crater rims, crests of buried or degraded crater rims, graben traces (certain and approximate), grooves, troughs, and impact-basin ring structures. Mapped location and surface features include pitted cones and secondary crater chains, respectively.

Ridges

We identified two types of positive-relief, ridge-like features in the map area. Wrinkle ridges are linear, asymmetric ridges and are ubiquitous throughout the map area, primarily on the terra units. These features generally have a north-south orientation. We mapped 76 ridge crests ranging in length from 6 to 27 km. An impact-basin ring represents the approximate location of a structural ring related to the formation of an ancient basin, such as Ladon and Holden basins in our map area. The basin ring locations are based on topographic remnants centered around an impact basin and correlation to low-calcium pyroxene signatures identified from CRISM data (Cartwright and Seelos, 2019).

Depressions

We mapped four types of depressions in the map area: graben trace, channel (fluvial), trough, and groove. A graben trace is a linear to curvilinear flat-floored depression bounded by two inward-facing normal faults that is too small for its faults to be mapped at map scale, typically <1 km in width. Graben traces are most commonly located in crater and basin fill units. They exhibit no preferred orientation, except within Ladon basin where they are arcuate and follow the basin edge. We mapped 240 graben that range in length from 900 m to 134 km.

A channel (fluvial) is a narrow, sinuous to branching depression with jagged margins that follows the topographic slope. We interpret the channels to be fluvial in origin, for example the channels and valleys that make up the Arda Valles system. All channels exhibit a radial flow direction that is consistent with transport downslope into Ladon basin. We mapped 217 channels that range from 576 m to 118 km in length.

A trough is a rounded to curvilinear depression found within Ladon basin. Troughs appear to be formed by collapse, subsidence, and (or) structural deformation of the surface. We mapped three troughs in our map area ranging in length from 29 to 72 km and having widths greater than 1 km.

A groove is a shallow linear depression with jagged margins in the highlands north of Ladon basin that may be fluvial and (or) structural in origin. Grooves appear similar to valleys in morphology but are perpendicular to valley flow direction and exhibit no sinuosity. We interpret grooves to be graben that were later modified by water flow after being breached by a valley. We mapped four grooves 10 to 28 km in length.

Scarps

A scarp crest is a topographically curving boundary that defines the margins and terminations of lobe-like landforms, such as along the west edge of Ladon basin. Scarp crests are steeper, longer, and have higher topography than ridge crests. We mapped 19 scarp crests that range in length from 1 to 140 km.

Crater Rims

We mapped crater rims for all craters 5 km and larger in diameter. We identified two types of crater rims: a "crest of crater rim" is an impact crater rim that clearly rises above the surrounding terrain and is well defined, and a "crest of buried or degraded crater rim" is an inferred crater rim that has been completely degraded or buried and does not have a visibly raised edge. We identified both exposed and buried crater rims throughout the map area. The largest crater rim we mapped is 40 km in diameter.

Pitted Cones

We identified one type of positive-relief, vent-like edifice within the map area that is mapped as a location feature. A pitted cone is a conical landform that contains a central pit or depression. HiRISE and CTX images show a smooth dark unit surrounding the pitted cone, consistent with a lava flow erupted from a vent. We mapped two pitted cones with diameters of 3 and 8 km that are adjacent to each other and occur along small fractures in southern Ladon basin.

Secondary Crater Chains

Secondary crater chains, mapped as surface features, are discontinuous chains of shallow, irregularly shaped craters that emanate radially from a larger impact structure. We interpreted them to have come from the south, most likely from Holden crater, although some of the more circular and smaller secondary craters could be from the 137-km-diameter Hale crater that is ~830 km to the south of the map area.

Age Determinations

We assessed relative ages of mapped units using stratigraphic relations and crater statistics. We compiled the latter in GIS using a subset of a global CTX mosaic (Dickson and others, 2018). We measured crater-rim diameters using CraterTools (Kneissl and others, 2011). The resolution of the CTX mosaic enabled confident definition of craters and we excluded obvious secondary craters when determining the crater size–frequency distributions and the interpretation of absolute-model ages.

We derived estimated absolute-model ages for each count from segments of the crater size–frequency plots for each unit that best match the expected production population using "pseudo-log" binned reverse cumulative histograms and Craterstats2 software (Michael and Neukum, 2010) (fig. 3, map sheet). The range of crater diameters that provide the best fit to the expected production function and the number of craters in this range are reported in table 1. We based estimated absolute-model ages on the chronology function of Hartmann and Neukum (2001) and production function from Ivanov (2001). The estimated absolute-model ages for all units are summarized in table 1. These absolute-model ages are consistent with observed superposition and crosscutting relations within the error bars of the crater counts and inform age relations shown in the Correlation of Map Units and Major Events (map sheet).

We assigned map units (described in the following subsections) to Martian epochs, as defined by Michael (2013), and accounted for (1) unit superposition relations observed and interpreted from mapping observations, which define the sequence of unit emplacement, as well as the (2) estimated absolute-model age derived from crater statistics (fig. 3). We also provided Martian epochs as defined by Hartmann and Neukum (2001) in table 1 to help correlate units to nearby maps where the epochs of Michael (2013) had not been used (for example, Irwin and Grant, 2013; Wilson and others, 2022). The occurrence of the Late Hesperian Holden crater ejecta and secondary craters (Mangold and others, 2012; Irwin and Grant, 2013) provides additional relative-age constraints within the map area.

Plateau and Highland Units

Crater statistics indicate the mountainous unit (Nm), terra 1 unit (Nt_1) and terra 2 unit (Ht_2) have estimated absolute-model ages of 3.9 (+0.02/–0.03) Ga (Middle Noachian), 3.8 (+0.03/–0.04) Ga (Late Noachian), and 3.6 (+0.03/–0.04) Ga (Early to Late Hesperian), respectively (fig. 3*A*; table 1), which are consistent with previous age estimates (for example, Schultz and others, 1982; Irwin and Grant, 2013).

Basin Fill Units

Having the largest crater diameters, basin fill 1 unit (HNb_1) and basin fill 2 unit (HNb_2) are estimated to have absolute-model ages of 3.8 (+0.08/–0.2) Ga and 3.8 (+0.06/–0.1) Ga, respectively (fig. 3*B*; table 1). We determined that these Late Noachian to Early Hesperian deposits were resurfaced in the Early to Late Hesperian (~3.6 Ga) on the basis of the best match to the expected production population at smaller diameter craters (fig. 3*B*; table 1). Basin fill 3 unit (HNb_3) has an estimated absolute-model age of 3.7 (+0.02/–0.03) Ga, corresponding to deposition in the Late Noachian to Early Hesperian. Basin fill 4 unit (AHb_4), light-toned layered unit (AHlb), and basin fill 5 unit (AHb_5) yield estimated model ages of ~3.3 Ga, corresponding to the Late Hesperian to Early Amazonian (fig. 3*C*; table 1). Based upon superposition relations, unit AHb_5 is younger than unit AHlb, which in turn is younger than unit AHb_4.

Crater, Valley, and Channel Units

Channel 1 unit (Nch_1) and channel 2 unit ($HNch_2$) have estimated absolute-model ages of 3.9 (+0.07/–0.1) Ga (Late Noachian) and 3.8 (+0.06/–0.1) Ga (Late Noachian to Early Hesperian), respectively (fig. 3*D*; table 1). The crater fill unit (Hcf) has an absolute-model age of 3.6 (+0.05/–0.07) Ga (fig. 3*D*; table 1), corresponding to Early to Late Hesperian. The light-toned crater floor unit (AHlc) has an absolute-model age of 2.5 (±0.5) Ga (Early Amazonian), but we extended its lower age into the Hesperian on the basis of the superposition of secondary craters from Holden crater that formed in the Hesperian. Similarly, the light-toned layered highland unit (AHlh) has an absolute-model age of 2.2 (±0.8) Ga, corresponding to the Early Amazonian, but, given that some of these deposits are related to the formation of Arda Valles in the Hesperian, we extended the lower age boundary

Table 1. Characteristics used to estimate absolute-model ages and associated epochs of geologic units in the map region.

[Combined unit areas and the crater diameter range that best fits the production function are used to estimate absolute model age (fig. 3). Associated epochs estimated from boundaries in Hartmann and Neukum (2001) and Michael (2013) using the Neukum system (Hartmann and Neukum, 2001; Ivanov, 2001). D range, best-fit crater diameter range; km, kilometer; km^2, square kilometer; Ga, giga-annum; Ma, mega-annum]

Unit name	Unit label	Combined unit area (km^2)	Best-fit crater D range (km)	Number of craters used in D range	Absolute-model age	Epoch (Hartmann and Neukum, 2001)	Epoch (Michael, 2013)
Volcanic Units							
Volcanic[a]	Av	187	0.175–0.4	27	580 (±100) Ma	Middle to Late Amazonian	Middle Amazonian
Chaotic Units							
Chaotic[a]	Act	638	0.35–2	12	1.1 (±0.3) Ga	Early to Middle Amazonian	Early to Middle Amazonian
Basin Fill Units							
Basin fill 5[b]	AHb_5	1,003	0.5–2.5	19	3.3 (+0.1/–0.3) Ga	Late Hesperian to Early Amazonian	Late Hesperian to Early Amazonian
Light-toned layered basin[b]	AHlb	262	0.35–2.5	14	3.3 (+0.1/–0.5)	Late Hesperian to Early Amazonian	Late Hesperian to Early Amazonian
Basin fill 4[b]	AHb_4	643	0.3–1.4	79	3.3 (+0.08/–0.1) Ga	Late Hesperian to Early Amazonian	Late Hesperian to Early Amazonian
Basin fill 3[c]	HNb_3	20,119	1.3–8	60	3.7 (+0.02/–0.03) Ga	Late Noachian to Early Hesperian	Late Noachian to Early Hesperian
Basin fill 2[c]	HNb_2	6,124	0.7–2	53	3.6 (+0.03/–0.04) Ga	Early to Late Hesperian	Early to Late Hesperian
			2–8	6	3.8 (+0.06/–0.1) Ga	Late Noachian	Late Noachian to Early Hesperian
Basin fill 1[c]	HNb_1	35,911	1.5–8	32	3.6 (+0.04/–0.05) Ga	Early to Late Hesperian	Early to Late Hesperian
			10–40	3	3.8 (+0.08/–0.2) Ga	Late Noachian	Late Noachian to Early Hesperian
Crater, Valley, and Channel Units							
Alluvial fan[d]	Af	142	0.3–0.7	11	2.5 (+0.6/–0.8) Ga	Late Hesperian to Early/ Middle Amazonian	Early Amazonian
Light-toned layered highland[d, e]	AHlh	109	0.3–0.7	7	2.2 (±0.8) Ga	Late Hesperian to Middle Amazonian	Early Amazonian
Light-toned crater floor[d, f]	AHlc	139	0.25–0.9	21	2.5 (±0.5) Ga	Late Hesperian to Early/ Middle Amazonian	Early Amazonian
Crater fill[d]	Hcf	3,724	1–6	14	3.6 (+0.05/–0.07) Ga	Early to Late Hesperian	Early to Late Hesperian
Channel 2[d]	$HNch_2$	158	0.6–1.3	5	3.8 (+0.06/–0.1) Ga	Late Noachian to Early Hesperian	Late Noachian to Early Hesperian
Channel 1[d]	Nch_1	256	0.7–4	3	3.9 (+0.07/–0.1) Ga	Middle to Late Noachian	Late Noachian
Plateau and Highland Units							
Terra 2[a]	Ht_2	11,754	1–8	47	3.6 (+0.03/–0.04) Ga	Early to Late Hesperian	Early to Late Hesperian
Terra 1[a]	Nt_1	90,210	7–35	22	3.8 (+0.03/–0.04) Ga	Late Noachian	Late Noachian
Mountainous[a]	Nm	12,701	2–17	44	3.9 (+0.02/–0.03) Ga	Middle Noachian	Middle Noachian

[a]Cumulative plot on fig. 3*A*.

[b]Cumulative plot on fig. 3*C*.

[c]Cumulative plot on fig. 3*B*.

[d]Cumulative plot on fig. 3*D*.

[e]Some formed during Arda Valles activity.

[f]Underlies secondary craters from Holden ejecta.

into the Hesperian. The alluvial fan unit (Af) is 2.5 (+0.6/–0.8) Ga (Early Amazonian), consistent with the timing of alluvial fan activity in and around eastern Ladon (Irwin and Grant, 2013) and Margaritifer basins (Wilson and others, 2022).

Chaotic Units

The chaotic terrain unit (Act) in the map area has an estimated absolute-model age of 1.1 (±0.3) Ga (fig. 3*A*; table 1). Unit Act corresponds to the Early to Middle Amazonian epochs but may be related to the formation of the Late Hesperian to Middle Amazonian chaotic terrain in nearby Margaritifer basin (Wilson and others, 2022).

Volcanic Units

A volcanic unit (Av), not previously mapped by others, has an estimated absolute-model age of 580 (±100) Ma (fig. 3*A*; table 1). Stratigraphic relations show this Middle Amazonian volcanic unit is younger than the basin fill 3 unit (HNb_3). The small area of unit Av (187 square kilometers [km^2]) makes the resulting absolute-model age less certain relative to larger map units; therefore, unit Av may be related to Late Hesperian to Amazonian volcanic vents adjacent to nearby Margaritifer basin (Wilson and others, 2022).

Geologic Summary

In this section, we summarize the geologic history of western Ladon basin, including northern Ladon Valles and the western highlands surrounding Ladon basin, based on the geologic unit, landform mapping, and stratigraphic determinations presented herein. This summary is portrayed graphically in the Correlation of Map Units and Major Events (map sheet).

Middle to Late Noachian Epochs

Both the Ladon and Holden impact basins formed prior to ~3.7–3.9 Ga (Irwin and Grant, 2013) and are perhaps as old as 4.17 Ga, when the martian dynamo was still active (Lillis and others, 2013). The basin-forming events produced an arcuate series of mountains, which we map as the mountainous unit (Nm), owing to the combination of initial crustal uplift followed by structural collapse. Our map area includes the remnants of two prominent rings of both Ladon and Holden basins that were identified by Cartwright and Seelos (2019) using a combination of topography and the presence of low-calcium pyroxene in these topographic features. Noachian landscape degradation, which included erosion and deposition of materials by impact, mass wasting, wind, and water, reduced these mountains in size and resulted in the unconformity that separates unit Nm from the terra 1 unit, Nt_1, that embays it. Only isolated massifs that represent the deeper Noachian bedrock outcrops exposed during the Holden and Ladon impacts remain at the time of mapping, and we mapped them and associated shedding debris as part of unit Nm, consistent with Irwin and Grant (2013). The mountainous structures and their associated topography controlled the flow of later flood channels and smaller fluvial valleys, which in turn influenced the depositional sites of phyllosilicate-bearing sediments within the highlands.

The terra 1 unit (Nt_1) is a widespread, smooth to rolling, cratered, and variably dissected surface between degraded impact craters. The geomorphic surface may have resulted from impact cratering, ejecta emplacement, prolonged weathering, and (or) erosion primarily by water and wind as evidenced by numerous valley systems and eolian ripples (Grant and Parker, 2002; Irwin and Grant, 2013). As described by Irwin and Grant (2013), unit Nt_1 incorporates a diverse assemblage of materials that likely includes fractured basaltic bedrock (Bandfield and others, 2000), impact ejecta, aqueously altered rocks (Murchie and others, 2007), and fluvially reworked sediments. We determined an estimated absolute-model age of 3.8 Ga for unit Nt_1, which is Late Noachian based upon the epochs of Michael (2013) (fig. 3; table 1). Irwin and Grant (2013) mapped a terra unit, HNt, that was dated Late Noachian to Early Hesperian; however, they did not distinguish between the older and younger terra units as was done here.

The presence of north-south-oriented wrinkle ridges in unit Nt_1 documents east-west compression after the unit was emplaced. The wrinkle ridges are mostly circumferential to Tharsis, west of the map area; a proposed origin is by contraction and faulting of plains materials associated with the formation of the Tharsis rise (Wise and others, 1979; Watters and Maxwell, 1983). Holden secondary craters and possibly smaller circular secondary craters from Hale crater are common across the unit. Craters range from well preserved (crater Golden) to highly degraded (craters Grójec, Sigli, and Shambe). We interpret the unit to be an undifferentiated combination of highland rocks and sediments, likely consisting of impact breccias, lava flows, and sedimentary deposits that underwent resurfacing sufficient to remove ejecta blankets and rims and to smooth topography, possibly by large-scale regional flooding events.

Late Noachian to Early Hesperian Epochs

Incision of the ULM mesoscale outflow channels dominates the Late Noachian to Early Hesperian epochs in the region (Parker and Pieri, 1985b; Grant and Parker, 2002; Irwin and Grant, 2013; Wilson and others, 2018). The Holden and Ladon basins imparted considerable structural and topographic influence on the course of the ULM system, with incised segments turning as they cross the basin rims to become radial to depositional-basin centers. Both Holden and Ladon multi-ringed impact basins most likely overflowed with water emanating from Argyre Planitia south of the map area. Clifford and Parker (2001) proposed that the water in Argyre Planitia was derived from meltwater from a southern polar ice cap. The initial discharge and resultant downstream flooding could have been significant and rapid because Ladon Valles contains multiple channels south of our map area, rather than a single confined channel. The initial flow through Ladon Valles during the Late Noachian carved out a broad, smooth to hummocky channel, unit Nch_1, with a sloping surface along its margins before flow coalesced and was confined to a narrower smooth, flat-lying channel, unit $HNch_2$. The smooth, flat-lying surface of unit $HNch_2$

is consistent with deposition of materials within the channel, rather than a solely erosional feature that would have produced a rougher, sloping surface; therefore, we mapped the Ladon Valles channels as distinct geologic units rather than linear features within unit Nt_1.

Our units Nch_1 and $HNch_2$ are the same units as units $HNch_1$ and $HNch_2$ in Irwin and Grant (2013), respectively, that continue to the south. Crater-age dating by Irwin and Grant (2013) for a much larger area of both their units than the area of the equivalent units in our map area showed the channel units range in age from Late Noachian to Early Hesperian. Our crater counts for this much smaller area of these two units yielded ages of Late Noachian for unit Nch_1 and Late Noachian to Early Hesperian for unit $HNch_2$, using the epochs of Michael (2013) (fig. 3; table 1). Holden secondary cratering disrupts both units, consistent with these units being older than Late Hesperian. Unit Nch_1 dissects unit Nt_1 and is dissected by the younger unit $HNch_2$. CRISM images of unit $HNch_2$ show the presence of Fe/Mg smectites in association with medium-toned polygonally fractured surfaces. Weitz and others (2022) interpreted these clay signatures to be from chemical alteration of unit $HNch_2$ by water in Ladon Valles.

The basin fill units HNb_1 and HNb_2 are inside the inner ring of Ladon basin that is defined by unit Nm (fig. 4, map sheet). Both basin fill units are bounded by an arcuate scarp, although younger impact craters and valleys have removed the scarp in some locations. The arcuate scarp that defines the boundary of unit HNb_1 shows it embays, and is thus younger than, unit Nm. Some of the valleys within unit Nt_1 continue into and dissect units HNb_1 and HNb_2 (fig. 4), which suggests that the basin fill units are contemporaneous or older than some of the fluvial modification that also affected unit Nt_1. Because the arcuate scarp that defines the contact between units HNb_1 and Nt_1 is still preserved, the degradation of unit HNb_1 must have been less than that on unit Nt_1 either because unit HNb_1 is younger than unit Nt_1 and (or) unit HNb_1 is more indurated compared to unit Nt_1. The north-south-oriented wrinkle ridges mapped throughout units Nt_1 and Ht_2 are only mapped in the northern part of unit HNb_1. Graben disrupt both units HNb_1 and HNb_2, indicating that extensional rather than compressional forces predominantly affected the basin units.

The main characteristics that distinguish unit HNb_1 from unit HNb_2 include a more sloping surface of unit HNb_2, which resulted in small ridges and gullies observed at the contact with unit HNb_3, and the presence of more circumferential graben within unit HNb_2. Unit HNb_2 embays and overlaps unit HNb_1, indicating that it is younger. Similarly, basin fill unit HNb_3 embays and overlies unit HNb_2, indicating unit HNb_2 is older. Thus, units HNb_1 and HNb_2 are constrained by stratigraphic relations to be younger than units Nm and Nt_1 but are older than unit HNb_3. Crater densities for units HNb_1 and HNb_2 yield an absolute-model age of 3.8 Ga for both basin units, which is Late Noachian to Early Hesperian from the epochs of Michael (2013) (fig. 3; table 1). Our crater counts indicate resurfacing events affected both units in the Early to Late Hesperian (fig. 3; table 1).

The arcuate scarp that defines the contact between units HNb_1 and Nt_1 could represent a flow margin that was scoured by fluvially derived sediments deposited within Ladon basin by the initial phase of a catastrophic flow in Ladon Valles. Alternatively, the scarp may have formed by tectonic activity (contraction) after deposition of the sediments within the basin. Similarly, unit HNb_2 could be a slightly younger and smaller fluvially derived deposit from a second pulse of water and sediments flowing through Ladon Valles into Ladon basin. The basin units could also be moderately to strongly indurated volcanic and (or) sedimentary materials that underwent tectonic activity (contraction) to produce the arcuate scarp.

We mapped an additional basin unit, HNb_3, with a relatively smooth, moderately cratered surface across much of the floors of Ladon basin and Ladon Valles. This unit is spatially extensive and dense with curvilinear graben. Our crater densities of unit HNb_3 in Ladon basin yielded an estimated absolute-model age of ~3.7 Ga (fig. 3; table 1) and imply emplacement in the Late Noachian to Early Hesperian, consistent with the same unit HNb_2 surfaces to the east mapped by Irwin and Grant (2013) and Wilson and others (2022). A few CRISM images that cover unit HNb_3 show that it contains Fe/Mg smectites that are associated with either medium-toned polygonally fractured surfaces or crater ejecta (Weitz and others, 2022). We suggest that possible origins for unit HNb_3 include erosion-resistant indurated sediments derived from the south that were transported by water flowing through Ladon Valles and (or) thin lava flows erupted within Ladon basin that were locally altered by water to form clays. The deposits could also contain moderately to strongly indurated eolian sediments.

Fluvial channels that formed during the Late Noachian to Early Hesperian dissected much of unit Nt_1 as water flowed downslope into Ladon basin, producing Arda Valles and other valley systems in the Noachis Terra highlands. The lack of fluvial deposits at the mouth of Arda Valles and on the floor of Ladon basin indicates that either the sediments were buried by younger basin units or that the sediments were thin and distributed across the basin floor. The relative timing of this valley-network formation in the map area is constrained by the depositional hiatus between unit Nt_1 and the Holden secondary craters that superpose many valleys, corresponding to the Late Noachian to Early Hesperian, although there are younger, smaller valleys discussed in the "Late Hesperian to Early Amazonian" section. The timing of valley formation within this area is concurrent with widespread gradation elsewhere on Mars (for example, Grant 1987, 2000; Grant and Schultz 1990, 1993), suggesting that valley formation was not caused by local endogenic processes but rather by limited runoff sourced by precipitation (Irwin and Grant, 2013) and precipitation-recharged groundwater sapping (Grant, 2000; Grant and Parker, 2002). The Ladon basin wall and ejecta provided high topographic slopes and minimal infiltration surfaces that maximized runoff and stream power, causing rapid incision and the development of valley systems like Arda Valles. As discussed in Grant and Parker (2002), either rainfall or melting snow could have provided the water for valley formation during this period on Mars.

Craters that formed during the Late Noachian and Early Hesperian (part of unit HNc_1) are now highly degraded with the ejecta completely eroded by wind and water or mantled by younger materials, and the rims are heavily modified by erosion. We interpreted the crater floor units as rocks and (or) sediments emplaced by mass wasting and (or) eolian, volcanic, and fluvial processes; the lack of primary structures inhibits a more definitive interpretation.

Early Hesperian to Late Hesperian Epochs

Holden crater was formed by a large impact during the Hesperian (Mangold and others, 2012; Irwin and Grant, 2013). Holden secondary cratering disrupts all units in our map area, except unit AHb_5. We mapped craters that formed during this period as unit Hc_2. These mostly complex craters (>15 km) exhibit terraces, central peaks and (or) rings, and (or) flat floors (see Melosh, 1989). The craters show moderate degrees of degradation, with some crater floors containing deposits emplaced by mass wasting and (or) eolian, volcanic, and fluvial processes. Unit Hc_2 craters exhibit minor relief above surrounding materials, and discontinuous, poorly exposed ejecta may be present.

We mapped a smooth crater fill unit (Hcf) along the floors of the larger impact craters. Possible origins for unit Hcf include moderately to strongly indurated volcanic or eolian fill materials. The origin and composition may vary between individual craters. Graben commonly disrupt the unit, suggesting contraction caused by cooling or intrusive volcanism beneath the crater (Bamberg and others, 2014). Alternative formation scenarios proposed for the fractured crater floors (mapped as both unit Hcf and chaotic unit Act within some craters) include deflation caused by collapse of an infill layer from drainage of either a surface lake (Sato and others, 2010) or a buried subice lake (Roda and others, 2017).

In the northern part of our map area, we identified a younger terra unit (Ht_2). Surfaces are relatively smooth over kilometers and are moderately cratered and variably dissected. The same north-south-oriented wrinkle ridges in unit Nt_1 are also present in unit Ht_2, as well as Holden secondary craters. However, valley systems do not occur in unit Ht_2. Crater densities indicated an estimated absolute-model age of 3.6 Ga (fig. 3; table 1). Superposition relations between units Nt_1 and Ht_2 confirm that unit Nt_1 is older. We interpret unit Ht_2 as moderately to strongly indurated volcanic, alluvial, and (or) eolian fill materials.

Late Hesperian to Early Amazonian Epochs

We mapped a fourth Ladon basin fill unit as unit AHb_4. The only physical difference between units HNb_3 and AHb_4 is that unit AHb_4 has undulating topography with the ridges appearing brighter in CTX images relative to the darker lower lying swales. The higher standing ridges, which are generally oriented north-south, consist of a partly stripped surface layer with a rougher, etched appearance compared to the more subdued and smoother dark surface between the ridges. We interpreted that the lower lying swales are darker and smoother because they retain a surficial mantle, possibly unit AHb_5, that has been eroded from the ridges. The undulating topography in unit AHb_4 could be the result of depositional or later erosional processes. The origin of the undulating topography relative to unit HNb_3 is unknown.

Crater statistics indicate that unit AHb_4 is 400 million years younger than unit HNb_3, although the two units could be contemporaneous because of the lack of embayment or superposition relations and the poor crater statistics for unit AHb_4 caused by the younger dark eolian materials filling the swales. Possible origins for unit AHb_4 include erosion-resistant, indurated sediments derived from the south that were transported by water flowing through Ladon Valles into Ladon basin and (or) thin lava flows that were erupted within Ladon basin that were subsequently tectonically deformed to produce the undulating appearance. The deposits could also contain moderately to strongly indurated eolian sediment, as evidenced by the darker fill in topographic lows between the ridges.

We mapped isolated, irregularly shaped outcrops located in northern Ladon Valles and southern Ladon basin as the light toned layered basin unit (AHlb), where layering is present in higher resolution images and the deposits appear light toned in visible wavelengths (for example, in HiRISE and CTX images). Layers are often 1 to 2 m thick, can be traced over tens of kilometers, and do not appear to truncate one another. Although the overall appearance of the deposits is light toned in visible data, close-up views of the deposits in HiRISE images show that there are some medium-toned layers interbedded with the light-toned layers. Outcrops of unit AHlb can show a massive bright layer commonly found along the base of the deposit, medium-toned layers dominating the middle portion of the deposit, and very bright layers near the top of the deposit (fig. 6, map sheet). The difference in reflectance between the bright and darker layers could identify variable source materials upstream or differences in grain sizes or diagenesis within the sediments (Weitz and others, 2022). The thickest deposit within our map area (fig. 6) occurs at the mouth of Ladon Valles and is ~60 m thick with ~40 individual layers visible within this outcrop. Some of the contacts between the base of unit AHlb and lower units are certain, for example, in Ladon Valles where unit AHlb overlies channel unit $HNch_2$. In other locations (for example, within Ladon basin) the base of AHlb is not observed and the contact with basin fill unit HNb_3 is uncertain. CRISM data indicate that the layered sediments contain Fe/Mg smectites, with some of these clays lacking an H_2O absorption band at 1.9 µm (Weitz and Bishop, 2012; Weitz and others, 2022). The clay mineralogy is consistent with weathering, transport, deposition, and (or) alteration by neutral pH rather than acidic fluids (Milliken and Bish, 2010).

Small outliers of light-toned layered deposits smaller than our map scale occur throughout Ladon basin and Ladon Valles, suggesting that these deposits were much greater in extent but have been eroded by the wind or buried beneath younger basin-fill material. We mapped unit AHlb, even where there was an extensive darker capping material covering much of the deposit, if we could identify outcrops of light-toned material exposed beneath the capping material, following mapping by Irwin and Grant (2013) for eastern Ladon Valles and Holden crater. The darker capping material was mapped as part of unit AHlb because we assumed that the light-toned layered deposit was situated directly beneath it. The unit has an estimated absolute-model age of 3.3 Ga from crater counts (fig. 3; table 1), but we mapped it as Late Hesperian to Early Amazonian because the unit is disrupted by Holden secondary cratering. The same unit was mapped as Late Hesperian by Irwin and Grant (2013). We interpreted the deposits to be weakly indurated and susceptible to eolian erosion, consistent with a fine grain size that could be either lacustrine sediments from a lake within Ladon basin that also filled portions of Ladon Valles or distal alluvial deposits at the mouth of Ladon Valles where it entered into the deeper Ladon basin.

We mapped several outcrops of light-toned layered deposits in the Noachis Terra highlands west of Ladon basin as unit AHlh (Weitz and others, 2013, 2019, 2022). The deposits within Arda Valles may have formed when water flow was blocked at the east end by topography associated with Cardona crater, which produced small basins where sediments could collect. We suggest that valley drainage into the basins and the associated deposition of the layered sediments during valley blockage likely continued until an outlet was established to the east that enabled incision of the deposits and drainage onto the lower lying floor of Ladon basin. An associated ~15-m-thick inverted channel within one of the valleys (lat −19.89° N., long 327.84° E.) is consistent with deposition in a closed basin, followed by erosion when an outlet valley was established. Evidence of point-bar migration is also preserved in the inverted channel and indicates repeated discharge (for example, Nanson, 1980).

Unit AHlh deposits farther north of Arda Valles may also represent sites where drainage along valleys that trend eastward became obstructed by topographic barriers (for example, the mountainous outcrops of unit Nm). Deposits within these basins contain numerous beds with variable colors and brightness, suggesting multiple episodes of deposition and (or) changing aqueous conditions over time. The valley systems that drain into basins incised and eroded older crustal materials (for example, units Nm and Nt_1) that became the source of the sediment. CRISM spectra extracted from the largest exposures of unit AHlh are consistent with Fe/Mg smectites (Weitz and others, 2022). Because of the small areal extent of the craters, we found it difficult to measure enough craters to obtain confident statistics to date the age of the unit. Using only seven craters (0.3–0.7 km diameter) covering an area of just 109 km^2, we determined an estimated absolute-model age of 2.2 Ga (fig. 3; table 1), which is Early Amazonian, using the epochs of Michael (2013). However, because some of the deposits formed at the same time as Arda Valles, they must extend into the Hesperian, which is why we gave the unit both a Hesperian and Amazonian age.

We also mapped an exposure of unit AHlh within a Holden secondary crater chain. We suggest that small valleys converged and breached the western walls of the secondary chain before depositing the ~40-m-thick layered sediment on the crater-chain floor (fig. 7, map sheet), indicating that the unit was deposited after Holden crater formed in the Hesperian. Because the layered deposit is situated above the crater floors, it is thickest at the mouth of the valleys where they breach the crater rim, and no other secondary craters along this same crater chain have either layered deposits within them or valleys that flow into them, we interpreted that unit AHlh was deposited by fluvial processes after these secondary craters formed. If the deposits were in the subsurface and exposed by the secondary craters scouring out the deposits, then we would not expect the layered deposits to rise above the crater floor elevation, which is what we observed. There are no CRISM images of these younger deposits, but HiRISE images show similar light-toned layered deposits to those observed in unit AHlh to the northeast where CRISM data detected the presence of Fe/Mg smectites (Weitz and others, 2019, 2022). Some of the younger outcrops of unit AHlh may have formed concurrently with light-toned layered clay-bearing deposits found nearby to the south in Eberswalde (Malin and Edgett, 2003; McKeown and Rice, 2011) and Holden craters (Grant and others, 2008; Milliken and Bish, 2010), which also have fluvial valleys dissecting the same unit Nt_1 and depositing sediments within craters. The fluvial activity may have been from precipitation and (or) snow melt across much of Margaritifer Terra during this time (Grant and Wilson, 2012; Mangold and others, 2012).

Exposures of the light-toned crater floor unit (AHlc) are mapped in the floors of a partially buried impact crater in Ladon basin and three craters in the Noachis Terra highlands southwest of Ladon basin. The brightness of the unit in HiRISE and CTX images varies from very bright to medium toned, depending upon the amount of overlying dark mantle and eolian debris, as well as the relative brightness of the surrounding terrain. The unit exhibits little or no layering, possibly because the exposures are too thin (<1–2 m) to show any layering that may exist within the deposit, which is how we differentiated it from the strata exposed in the layered light-toned deposits of units AHlb and AHlh. We distinguished unit AHlc from the crater rims, because it is generally brighter in THEMIS nighttime IR images and darker in THEMIS daytime IR images, exhibits polygonal meter-scale fracturing in HiRISE images, lacks the numerous small craters observed along the crater rims, and is bright in HiRISE and CTX images even though it is flat-lying and does not face the sun. In contrast, the adjacent crater rims are high-standing, heavily cratered, and only appear bright in THEMIS daytime IR, HiRISE, and CTX images if they are sun facing (for example, located on the east side of the crater rim).

Several outcrops of unit AHlc occur within a partially buried 38-km-diameter crater in northern Ladon basin, centered at lat −17.4° N., long 328.58° E. These are best seen beneath eroded ejecta from Holden secondary craters or where erosion has removed the dark, thin capping material, which could be small exposures of unit AHb_5. We mapped these small outcrops of unit AHlc but recognize that they could also be a thin bed from the light-toned layered deposits observed in southern Ladon basin and Ladon Valles (unit AHlb).

Three impact craters along the Noachis Terra highlands southwest of Ladon basin have unit AHlc on their floors. The unit occurs as small outcrops of rugged knobs and blocks (at meters to hundreds of meters in length). Unit AHlc is characterized by light-toned material that has limited or no layering, which is why we distinguished it from the light-toned layered deposits of unit AHlh. There are no CRISM images that cover these crater deposits, so we were not able to determine their composition. The deposits could be thinner materials of unit AHlh or crater floor material altered by water ponding inside each crater, although there are no obvious valleys that enter these craters, so the source of water to cause the alteration is unknown. Our crater counting produced an estimated absolute age of 2.2 Ga, which corresponds to the Early Amazonian in the epochs of Michael (2013) (fig. 3; table 1). We extended the age of the unit to Late Hesperian because Holden secondary craters and their ejecta disrupt and cover portions of the deposit in Ladon basin.

Basin fill unit AHb_5 is characterized by a smooth (over kilometers), low-relief surface. We mapped this unit as the youngest basin fill unit within Ladon basin. The initiation of deposition of unit AHb_5 and its stratigraphic relation to the units beneath it are certain, shown by a solid line along the base of the unit box in the Correlation of Map Units and Major Events (map sheet). Smaller, lower relief outliers that are below mapping resolution (<5 km) are

common across the Ladon basin floor. We interpreted the patchy and discontinuous nature of unit AHb_5, especially small outcrops found on the floors of impact craters and other depressions, to indicate that the deposit was once broader and more continuous in areal extent but has been removed over time by erosion. Many outcrops of unit AHb_5 appear as mesas with steep edges (fig. 5, map sheet), suggesting that it is composed of lithified or indurated rather than unconsolidated materials. The unit retains craters but has fewer craters than other basin fill units that it overlies. The deposits that we mapped are all darker in HiRISE and CTX images relative to the adjacent units. Unit AHb_5 overlies basin fill units HNb_3 and AHb_4, as well as basin and channel units AHIb, Nch_1, and $HNch_2$. Unit AHb_5 also overlies Holden secondary craters, consistent with an age of Late Hesperian or younger. Crater counts yielded an estimated absolute-model age of 3.3 Ga (fig. 3; table 1), indicating a Late Hesperian to Early Amazonian age, using the epochs of Michael (2013). The unit could be lithified eolian debris, lava flows, or late-stage sediments from Ladon Valles.

Craters that formed during this time were mapped as unit AHc_3 and are morphologically fresh, with elevated rims and ejecta relative to surrounding materials. A well-defined, continuous ejecta blanket is often present. Layered and lobate ejecta morphologies are well preserved and pervasive. Some crater floors may contain deposits of impact melt and (or) impact-generated fine-grained materials.

Early to Middle Amazonian Epochs

Sloping or cone-shaped deposits that we interpreted to be alluvial fans (unit Af) are mapped in two impact craters in our map area. The alluvial fans are similar in morphology to those seen elsewhere in Margaritifer Terra (for example, Grant and Wilson, 2011, 2012; Wilson and others, 2021, 2022; Irwin and Grant, 2013). The fans cover much of the floor of the 24-km-diameter Alnif crater (lat −15.1° N., long 328.9° E.). We interpreted these deposits as alluvial fans emplaced by fluvial activity with little to no evident contribution from debris flows given the lack of boulders visible in HiRISE images and fan-surface gradients that support construction by mostly gravel size and smaller sediment (Moore and Howard, 2005; Grant and Wilson, 2011). For the two occurrences of unit Af in our map area, we determined an estimated absolute-model age of 2.5 Ga from crater counts, which is Early Amazonian based upon the epochs of Michael (2013). By combining the crater size–frequency distributions for a large subset of the alluvial fans in Margaritifer Terra, Grant and Wilson (2011) derived a Late Hesperian to Early Amazonian age for the formation of the alluvial fans. Consequently, unit Af could also have a Late Hesperian age, although it is not disrupted by Holden secondary cratering in our map area like units AHIh and AHIc so we did not extend it into the Hesperian like we did for these other units. Unit Af is emplaced on, and is therefore younger than, crater floor unit Hcf and crater 3 unit AHc_3. We interpreted unit Af as the youngest fluvial unit in the map area (although it could also be contemporaneous with the fluvial activity that deposited highland unit AHIh in the Holden secondary craters). The water-driven activity that produced these alluvial fans may be related to precipitation, perhaps as snowfall, which accumulated in crater-rim alcoves and (or) depressions and later melted to produce runoff (Grant and Wilson, 2012).

We identified chaotic material that we mapped as unit Act inside several unnamed craters in our map area. The unit has been tectonically deformed, resulting in irregular patches of closely spaced knobs or irregular blocks of similar heights, where less than 50 percent of the original surface is still intact. The crater interior margins are generally more disrupted than the crater centers. Possible formation processes include localized inflation by volcanism and (or) deflation of the surface caused by collapse of an infill layer within a crater from drainage of either a surface lake (Sato and others, 2010) or a buried subice lake (Roda and others, 2017). We also mapped a small outcrop of chaotic material and associated graben in the northwest part of our map area as unit Act. This outcrop is part of a broader area of chaos just south of Eos Chasma and suggests collapse, perhaps caused by withdrawal of material at depth in this area. Additionally, this area is at the distal end of Tigre Valles (fig. 1), just northwest of our map area. Water from Tigre Valles may have caused erosion and deflation of the surface that resulted in unit Act forming in the terra unit here. The estimated absolute-model age derived from our crater counts is 1.1 Ga (fig. 3; table 1), indicating an Early to Middle Amazonian age for unit Act.

We identified and mapped two cones with central depressions at the southern edge of Ladon basin. We mapped these cones and the associated dark material around them as volcanic unit Av. Based on CTX and HiRISE images, this unit appears smooth (fig. 8, map sheet). We interpreted the dark material to be lava flows erupted from the volcanic cones, but the morphology is also similar to unit AHb_5. Although the small area (187 km^2) used in this age estimate greatly increases the error range, the estimated absolute-model age of the unit based upon crater counts is 580 mega-annum (Ma) (table 1), which makes this the youngest unit within our map area. Fractures that are mapped as graben intersect both volcanic cones and may be evidence of subsurface dikes that fed the volcanic eruption. The volcanic cones likely resulted from localized magmatic activity that could have used zones of weakness along the south edge of the Ladon impact basin. This volcanic activity in Ladon basin would have been contemporaneous with similar volcanic units mapped along the margin of Margaritifer basin, northeast of the map area (fig. 1) (Wilson and others, 2022). Alternatively, the cones may have formed by mud volcanism (Skinner and Mazzini, 2009) caused by the volatile-rich sediments that would have been emplaced here from water flow through Ladon Valles and into Ladon basin.

The final geologic activity in the map area created a variable veneer associated with locally occurring impacts and redistribution of fine materials by the wind.

Acknowledgments

This work was sponsored by the National Aeronautics and Space Administration (NASA) Planetary Geology and Geophysics Program grant NNX13AM81G. The authors thank Corey Fortezzo and Marc Hunter of the U.S. Geological Survey (USGS) for assistance with GIS mapping techniques and Jim Skinner for serving as the map coordinator.

References Cited

Baker, V.R., 1982, The channels of Mars: Austin, University of Texas Press, 198 p.

Bamberg, M., Jaumann, R., Asche, H., Kneissl, T., and Michael, G.G., 2014, Floor-fractured craters on Mars—Observations and origin: Planetary Space Science, v. 98, p. 146–162.

Bandfield, J.L., Hamilton, V.E., and Christensen, P.R., 2000, A global view of Martian surface compositions from MGS-TES: Science, v. 287, p. 1626–1630. [Also available at https://doi.org/10.1126/science.287.5458.1626.]

Boothroyd, J.C., 1983, Fluvial drainage systems in the Ladon basin area, Margaritifer Sinus area, Mars: Geological Society of America Abstract with Programs, v. 15, p. 530.

Cabrol, N.A., Wynn-Williams, D.D., Crawford, D.A., and Grin, E.A., 2001, Recent aqueous environments in Martian impact craters—An astrobiological perspective: Icarus, v. 154, p. 98–112.

Carr, M.H., 1981, The surface of Mars: New Haven, Conn., Yale University Press, 232 p.

Cartwright, S.F.A., and Seelos, K.D., 2019, New ring structure estimates of Ladon basin, Mars, from mafic mineral mapping with CRISM [abs.], *in* Lunar and Planetary Science Conference, 50th, The Woodlands, Tex., March 18–22, 2019, Program and Abstracts: Lunar and Planetary Science Institute, abstract no. 2755.

Christensen, P.R., Jakosky, B.M., Kieffer, H.H., Malin, M.C., McSween, H.Y., Jr., Nealson, K., Mehall, G.L., Silverman, S.H., Ferry, S., Caplinger, M., and Ravine, M., 2004, The Thermal Emission Imaging System (THEMIS) for the Mars 2001 Odyssey Mission: Space Science Reviews, v. 110, p. 85–130.

Clifford, S.M., and Parker, T.J., 2001, The evolution of the Martian hydrosphere—Implications for the fate of a primordial ocean and the current state of the northern plains: Icarus, v. 154, p. 40–79.

Dickson, J.L., Kerber, L.A., Fassett, C.I, and Ehlmann, B.L., 2018, A global, blended CTX mosaic of Mars with vectorized seam mapping—A new mosaicking pipeline using principles of non-destructive image editing [abs.], *in* Lunar and Planetary Science Conference, 49th, The Woodlands, Tex., March 19–23, 2018, Program and Abstracts: Lunar and Planetary Science Institute, abstract no. 2480.

Fassett, C.I., and Head, J.W., 2011, Sequence and timing of conditions on early Mars: Icarus, v. 211, p. 1204–1214. [Also available at https://doi.org/10.1016/j.icarus.2010.11.014.]

Federal Geographic Data Committee [prepared for the Federal Geographic Data Committee by the U.S. Geological Survey], 2006, FGDC digital cartographic standard for map symbolization: Reston, Va., Federal Geographic Data Committee Document Number FGDC-STD-013-2006, 290 p., 2 plates.

Fergason, R.L, Hare, T.M., and Laura, J., 2018, HRSC and MOLA blended digital elevation model at 200m v2: U.S. Geological Survey, Astrogeology Science Center, Planetary Data System Annex. [Available online at https://astrogeology.usgs.gov/search/map/Mars/Topography/HRSC_MOLA_Blend/Mars_HRSC_MOLA_BlendDEM_Global_200mp_v2.lbl.]

Fergason, R.L., Lee, E.M., Weller, L., 2013, THEMIS geodetically controlled mosaics of Mars [abs.], *in* Lunar and Planetary Science Conference, 44th, The Woodlands, Tex., March 18–22, 2013, Program and Abstracts: Lunar and Planetary Science Institute, abstract no. 1642.

Grant, J.A., 1987, The geomorphic evolution of eastern Margaritifer Sinus, Mars in advances in planetary geology: National Aeronautics and Space Administration, Technical Memorandum 89871, 268 p.

Grant, J.A., 2000, Valley formation in Margaritifer Sinus, Mars, by precipitation-recharged ground-water sapping: Geology, v. 28, p. 223–226.

Grant, J.A., Buczkowski, D., Irwin, R.P., III, and Siebach, K., 2010b, A lake in Uzboi Vallis and implications for Late Noachian climate on Mars [abs.], *in* Lunar and Planetary Science Conference, 41st, The Woodlands, Tex., March 1–5, 2010, Program and Abstracts: Lunar and Planetary Science Institute, abstract no. 1834.

Grant, J.A., Irwin, R.P., III, Grotzinger, J.P., Milliken, R.E., Tornabene, L.L., McEwen, A.S., Weitz, C.M., Squyres, S.W., Glotch, T.D., and Thomson, B.J., 2008, HiRISE imaging of impact megabreccia and sub-meter aqueous strata in Holden Crater, Mars: Geology, v. 36, p. 195–198. [Also available at https://doi.org/10.1130/G24340A.1.]

Grant, J.A., Irwin, R.P., III, and Wilson, S.A., 2010a, Aqueous depositional settings in Holden crater, Mars, *in* Cabrol, N.A., and Grin, E.A., eds., Lakes on Mars: Oxford, UK, Elsevier.

Grant, J.A., and Parker, T.J., 2002, Drainage evolution of the Margaritifer Sinus region, Mars: Journal of Geophysical Research, v. 107. [Also available at https://doi.org/10.1029/2001JE001678.]

Grant, J.A., and Schultz, P.H., 1990, Gradational epochs on Mars—Evidence from west-northwest of Isidis basin and Electris: Icarus, v. 84, p. 166–195.

Grant, J.A., and Schultz, P.H., 1993, Degradation of selected terrestrial and Martian impact craters: Journal of Geophysical Research, v. 98, no. E6, p. 11025–11042.

Grant, J.A., and Wilson, S.A., 2011, Late alluvial fan formation in southern Margaritifer Terra, Mars: Geophysical Research Letters, v. 38, no. 8, https://doi.org/10.1029/2011GL046844.

Grant, J.A., and Wilson, S.A., 2012, A possible synoptic source of water for alluvial fan formation in southern Margaritifer Terra, Mars: Planetary Space Science. [Also available at https://doi.org/10.1016/j.pss.2012.05.020.]

Greeley, R., and Batson, R., eds., 1990, Planetary mapping: Cambridge, MA, Cambridge University Press, 296 p.

Hartmann, W.K., and Neukum, G., 2001, Cratering chronology and the evolution of Mars: Space Science Reviews, v. 96, p. 165–194.

Hiesinger, H., and Head, J.W., III, 2002, Topography and morphology of the Argyre basin, Mars—Implications for its geologic and hydrologic history: Planetary and Space Science, v. 50, p. 939–981.

Irwin, R.P., III, and Grant, J.A., 2009, Chapter 11—Large basin overflow floods on Mars, *in* Burr, D.M., Baker, V.R., and Carling, P.A., eds., Megafloods on Earth and Mars: Cambridge, U.K., University Press, p. 209–224.

Irwin, R.P., III, and Grant, J.A., 2013, Geologic map of MTM −15027, −20027, −25027 and −25032 quadrangles, Margaritifer Terra region of Mars: U.S. Geological Survey

Scientific Investigations Map 3209, scale 1:1,000,000, https://doi.org/10.3133/sim3209.
Ivanov, B.A., 2001, Mars/Moon cratering ratio estimates: Space Science Review, v. 96, p. 87–104.
Jones, A.P., McEwen, A.S., Tornabene, L.L., Baker, V.R., Melosh, H.J., and Berman, D.C., 2011, A geomorphic analysis of Hale crater, Mars—The effects of impact into ice-rich crust: Icarus, v. 211, p. 259–272.
Kneissl, T., van Gasselt, S., and Neukum G., 2011, Map-projection-independent crater size-frequency determination in GIS environments—New software tool for ArcGIS: Planetary Space Science, v. 59, p. 1243–1254. [Also available at https://doi.org/10.1016/j.pss.2010.03.015.]
Lewis, K.W., and Aharonson, O., 2006, Stratigraphic analysis of the distributary fan in Eberswalde crater using stereo imagery: Journal of Geophysical Research, v. 111, no. E06001. [Also available at https://doi.org/10.1029/2005JE002558.]
Lillis, R.J., Robbins, S., Manga, M., Halekas, J.S., and Frey, H.V., 2013, Time history of the Martian dynamo from crater magnetic field analysis: Journal of Geophysical Research, v. 118, p. 1488–1511.
Malin, M.C., 1976, Nature and origin of intercrater plains on Mars, *in* Studies of the surface morphology of Mars: Pasadena, California Institute of Technology, Ph.D. dissertation.
Malin, M.C., Bell, J.F., III, Cantor, B.A., Caplinger, M.A., Calvin, W.M., Clancy, R.T., Edgett, K.S., Edwards, L., Haberle, R.M., James, P.B., Lee, S.W., Ravine, M.A., Thomas, P.C., and Wolff, M.J., 2007, Context Camera investigation on board the Mars Reconnaissance Orbiter: Journal of Geophysical Research, v. 112, no. E05S04. [Also available at https://doi.org/10.1029/2006JE002808.]
Malin, M.C., and Edgett, K.S., 2001, Mars Global Surveyor Mars Orbiter Camera—Interplanetary cruise through primary mission: Journal of Geophysical Research, v. 106, p. 23429–23570.
Malin, M.C., and Edgett, K.S., 2003, Evidence for persistent flow and aqueous sedimentation on early Mars: Science, v. 302, p. 1931–1934.
Mangold, N., Kite, E.S., Kleinhans, M.G., Newsom, H., Ansan, V., Hauber, E., Kraal, E., Quantin, C., and Tanaka, K., 2012, The origin and timing of fluvial activity at Eberswalde crater, Mars: Icarus, v. 220, no. 2, p. 530–551.
McEwen, A.S., Eliason, E.M., Bergstrom, J.W., Bridges, N.T., Hansen, C.J., Delamere, W.A., Grant, J.A., Gulick, V.C., Herkenhoff, K.E., Keszthelyi, L., Kirk, R.L., Mellon, M.T., Squyres, S.W., Thomas, N., and Weitz, C.M., 2007, Mars Reconnaissance Orbiter's High Resolution Imaging Science Experiment (HiRISE): Journal of Geophysical Research, v. 112, no. E05S02. [Also available at https://doi.org/10.1029/2005JE002605.]
McKeown, N.K, and Rice, M.S., 2011, Detailed mineralogy of Eberswalde Crater [abs.], *in* Lunar and Planetary Science Conference, 42d, The Woodlands, Tex., March 7–11, 2011, Program and Abstracts: Lunar and Planetary Science Institute, abstract no. 2450.
Melosh, H.J., 1989, Impact cratering: New York, Oxford University Press, 245 p.
Michael, G.G., 2013, Planetary surface dating from crater size-frequency distribution measurements—Multiple resurfacing episodes and differential isochron fitting: Icarus, v. 226, p. 885–890. [Also available at https://doi.org/10.1016/j.icarus.2013.07.004.]
Michael, G.G., and Neukum, G., 2010, Planetary surface dating from crater size–frequency distribution measurements—Partial resurfacing events and statistical age uncertainty: Earth and Planetary Science Letters, v. 294, no. 3-4, p. 223–229. [Also available at https://doi.org/10.1016/j.epsl.2009.12.041.]
Milliken, R.E., and Bish, D.L., 2010, Sources and sinks of clay minerals on Mars: Philosophical Magazine, p. 1478–6443. [Also available at https://doi.org/10.1080/14786430903575132.]
Moore, J.M., and Howard, A.D., 2005, Large alluvial fans on Mars: Journal of Geophysical Research, v. 110, no. E04005. [Also available at https://doi.org/10.1029/2004JE002352.]
Murchie, S., Arvidson, R., Bedini, P., Beisser, K., Bibring, J.-P., Bishop, J., Boldt, J., Cavender, P., Choo, T., Clancy, R.T., Darlington, E.H., Des Marais, D., Espirit R., Fort, D., Green, R., Guinness, E., Hayes, J., Hash, C., Heffernan, K., Hemmler, J., Heyler, G., Humm, D., Hutcheson, J., Izenberg, N., Lee, R., Lees, J., Lohr, D., Malaret, E., Martin, T., McGovern, J.A., McGuire, P., Morris, R., Mustard, J., Pelkey, S., Rhodes, E., Robinson, M., Roush, T., Schaefer, E., Seagrave, G., Seelos, F., Silverglate, P., Slavney, S., Smith, M., Shyong, W.-J., Strohbehn, K., Taylor, H., Thompson, P., Tossman, B., Wirzburger, M., and Wolff, M., 2007, Compact Reconnaissance Imaging Spectrometer for Mars (CRISM) on Mars Reconnaissance Orbiter (MRO): Journal of Geophysical Research, v. 112, no. E05S03. [Also available at https://doi.org/10.1029/2006JE002682.]
Murchie, S.L., Mustard, J.F., Ehlmann, B.L., Milliken, R.E., Bishop, J.L., McKeown, N.K., Eldar, Z., Seelos, F.P., Buczkowski, D.L., Wiseman, S.M., Arvidson, R.E., Wray, J.J., Swayze, G., Clard, R.N., Des Marais, D.J., McEwen, A.S., and Bibring, J.-P., 2009, A synthesis of Martian aqueous mineralogy after 1 Mars year of observations from the Mars Reconnaissance Orbiter: Journal of Geophysical Research, v. 114, no. E00D06. [Also available at https://doi.org/10.1029/2009JE003342.]
Nanson, G.C., 1980, Point bar and floodplain formation of the meandering Beatton River, northeastern British Columbia, Canada: Sedimentology, v. 27, p. 3–29. [Also available at https://doi.org/10.1111/j.1365-3091.1980.tb01155.x.]
Parker, T.J., and Pieri, D.C., 1985a, Geomorphology and geology of the southwestern Margaritifer Sinus and Argyre regions of Mars—I. Geological and geomorphological overview, *in* Reports of planetary geology and geophysics program—1984: Washington, D.C., National Aeronautics and Space Administration (NASA) Technical Memorandum 87563, p. 361–363.
Parker, T.J., and Pieri, D.C., 1985b, Geomorphology and geology of the southwestern Margaritifer Sinus and Argyre regions of Mars—II. Crater size-frequency distribution curves and geomorphic unit ages, *in* Reports of planetary geology and geophysics program—1984: Washington, D.C., National Aeronautics and Space Administration, Technical Memorandum 87563, p. 364–366.
Pondrelli, M., Baliva, A., Di Lorenzo, S., Marinangeli, L., and Rossi, A.P., 2005, Complex evolution of paleolacustrine systems on Mars—An example from the Holden crater: Journal of Geophysical Research, v. 110, no. 2004JE002335.
Pondrelli, M.A., Rossi, A.P., Marinangeli, L., Hauber, E., Gwinner, K., Baliva, A., and Di Lorenzo, S., 2008, Evolution and depositional environments of the Eberswalde fan delta, Mars: Icarus, v. 197, p. 429–451. [Also available at https://doi.org/10.1016/j.icarus.2008.05.018.]

Rice, M.S., Gupta, S., Bell, J.B., III, and Warner, N.H., 2011, Influence of fault-controlled topography on fluvio-deltaic sedimentary systems in Eberswalde crater, Mars: Geophysical Research Letters, v. 38. [Also available at https://doi.org/10.1029/2011GL048149.]

Robbins, S.J., and Hynek, B.M., 2012, Revising the earliest recorded impact history of Mars and implications for the late heavy bombardment [abs.], *in* Workshop on the Early Solar System Impact Bombardment II, Houston, Tex., February 1–3, 2012, Program and Abstracts: Lunar and Planetary Science Institute, abstract no. 4309.

Roda, M., Marketos, G., Westerweel, J., and Govers, R., 2017, Morphological expressions of crater infill collapse—Model simulations of chaotic terrains on Mars: Geochemistry, Geophysics, Geosystems, v. 18, p. 3687–3699, https://doi.org/10.1002/2017GC006933.

Sato, H., Kurita, K., and Baratoux, D., 2010, The formation of floor-fractured craters in Xanthe Terra: Icarus, v. 201, no. 1, p. 248–264.

Saunders, R.S., 1979, Geologic map of the Margaritifer Sinus quadrangle of Mars: U.S. Geological Survey, Miscellaneous Investigations Series Map I–1144.

Schultz, P.H., Schultz, R.A., and J. Rogers, J., 1982, The structure and evolution of ancient impact basins on Mars: Journal of Geophysical Research, v. 87, p. 9803–9820.

Scott, D.H., and Tanaka, K.L., 1986, Geologic map of the western equatorial region of Mars: U.S. Geological Survey Miscellaneous Investigations Series–1802–A.

Skinner, J.A., Jr., Black, S.R., Buban, H.C., Fortezzo, C.M., Gaither, T.A., Huff, A.E., and Hunter, M.A., 2022, Planetary geologic map protocol—2022: U.S. Geological Survey Techniques and Methods 11–B13, 28 p., https://doi.org/10.3133/tm11B13.

Skinner, J.A., Jr., and Mazzini, A., 2009, Martian mud volcanism—Terrestrial analogs and implications for formational scenarios: Marine and Petroleum Geology, v. 26, no. 9, p. 1866–1878.

Smith, D.E., Zuber, M.T., Frey, H.V., Garvin, J.B., Head, J.W., Muhleman, D.O., Pettengill, G.H., Phillips, R.J., Solomon, S.C., Zwally, H.J., Banerdt, W.B., Duxbury, T.C., Golombek, M.P., Lemoine, F.G., Neumann, G.A., Rowlands, D.D., Aharonson, O., Ford, P.G., Ivanov, A.B., McGovern, P.J., Abshire, J.B., Afzal, R.S., and Sun, X., 2001, Mars Orbiter Laser Altimeter (MOLA)—Experiment summary after the first year of global mapping of Mars: Journal of Geophysical Research, v. 106, p. 23689–23722.

Tanaka, K.L., Moore, H.J., Schaber, G.G., Chapman, M.G., Stofan, E.R., Campbell, D.B., Davis, P.A, Guest, J.E., McGill, G.E., Rogers, P.G., Saunders, R.S., and Zimbelman, J.R., 1994, The Venus Geologic Mappers' Handbook: U.S. Geological Survey Open-File Report 94–438, 66 p.

Tanaka, K., Skinner, J.A., Jr., Dohm, J.M., Irwin, R.P., III, Kolb, E.J., Fortezzo, C.M., Platz, T., Michael, G.G., and Hare, T.M., 2014, Geologic map of Mars: U.S. Geological Survey Scientific Investigations Map 3292.

Tanaka, K.L., Skinner, J.A, Jr., and Hare, T.M., 2011, Planetary geologic mapping handbook—2011: U.S. Geological Survey, unpublished handbook, 24 p. [Available online at https://astropedia.astrogeology.usgs.gov/download/Docs/Mappers/PGM_Handbook_2011.pdf.]

Thomas, R.J., Hynek, B.M., Osterloo, M.M., and Kierein-Young, K.S., 2017, Widespread exposure of Noachian phyllosilicates in the Margaritifer region of Mars—Implications for paleohydrology and astrobiological detection: Journal of Geophysical Research; Planets, v. 122, no. 3, https://doi.org/10.1002/2016JE005183.

Watters, T.R., and Maxwell, T.A., 1983, Crosscutting relations and relative ages of ridges and faults in the Tharsis region of Mars: Icarus, v. 56, no. 2, p. 278–298.

Weitz, C.M., and Bishop, J.L., 2012, Investigation of layered sediments at a proposed future Mars landing site in Ladon Valles [abs.], *in* Lunar and Planetary Science Conference, 43d, The Woodlands, Tex., March 19–23, 2012, Program and Abstracts: Lunar and Planetary Science Institute, abstract no. 1243.

Weitz, C.M., Bishop, J.L., and Grant J.A., 2019, Analysis of clay deposits in and around Ladon Basin and Ladon Valles [abs.], *in* Lunar and Planetary Science Conference, 50th, The Woodlands, Tex., March 18–22, 2019, Program and Abstracts: Lunar and Planetary Science Institute, abstract no. 1929.

Weitz, C.M., Bishop, J.L., Grant, J.A., Wilson, S.A., Irwin, R.P., Saranathan, A.M., Itoh, Y., Parente, M., 2022, Clay sediments derived from fluvial activity in and around Ladon basin, Mars: Icarus, v. 384, https://doi.org/10.1016/j.icarus.2022.115090.

Weitz, C.M., Grant, J.A., Irwin, R.P., III, and Wilson-Purdy, S.A., 2013, Sedimentary deposits associated with small upland basins around Ladon Basin [abs.], *in* Lunar and Planetary Science Conference, 44th, The Woodlands, Tex., March 18–22, 2013, Program and Abstracts: Lunar and Planetary Science Institute, abstract no. 2081.

Werner, S.C., 2008, The early Martian evolution—Constraints from basin formation ages: Icarus, v. 195, p. 45–60. [Also available at https://doi.org/10.1016/j.icarus.2007.12.008.]

Wilson, S.A., Grant, J.A., Howard, A.D., and Buczkowski, D.L., 2018, The nature and origin of deposits in Uzboi Vallis on Mars: Journal of Geophysical Research; Planets, v. 123, p. 1842–1862, https://doi.org/10.1029/2017JE005508.

Wilson, S.A., Grant, J.A., and Williams, K.K., 2022, Geologic map of MTM −10022 and −15022 quadrangles, Morava Valles and Margaritifer basin, Mars: U.S. Geological Survey Scientific Investigations Map 3489, 1 sheet, 11 p. pamphlet, https://doi.org/10.3133/sim3489.

Wilson, S.A., Morgan, A.M., Howard, A.D., and Grant, J.A., 2021, The global distribution of craters with alluvial fans and deltas on Mars: Geophysical Research Letters, v. 48, https://doi.org/10.1029/2020GL091653.

Wise, D.U., Golombek, M.P., and McGill, G.E., 1979, Tharsis province of Mars—Geologic sequence, geometry, and a deformation mechanism: Icarus, v. 38, no. 3, p. 456–472.